Reactant Selectivity and Regiospecificity in the Catalytic Oxidation of Alkanes on Metal-Substituted Aluminophosphates

Björn Modén,[†] Bi-Zeng Zhan,[†] Jihad Dakka,[‡] José G. Santiesteban,[‡] and Enrique Iglesia*[,†]

Department of Chemical Engineering, University of California at Berkeley, Berkeley, California 94720 and Corporate Strategic Research, ExxonMobil Research and Engineering Co., Route 22 East, Annandale, New Jersey 08801

Received: May 10, 2006; In Final Form: November 2, 2006

The rate of *n*-hexane reactions with O_2 increased in parallel with the concentration of hexyl hydroperoxide (ROOH) intermediates and with the number of Mn_{redox} sites in microporous MnAPO-5 and MnAPO-18 catalysts. These data confirmed the catalytic nature of oxidation pathways and the mechanistic resemblance between *n*-alkane and cycloalkane oxidation pathways. Cyclohexane oxidation turnover rates were higher on MnAPO-5 than on MnAPO-18, because small channels in the latter inhibit contact between reactants and Mn active centers. In contrast, *n*-hexane oxidation turnover rates (per redox-active Mn center) were similar on MnAPO-5 and MnAPO-18, because smaller *n*-hexane reactants diffuse rapidly and contact active sites in both microporous structures. MnAPO-18 is able to select reactants based on their size, but no regiospecificity was detected on MnAPO-18 or MnAPO-5 for *n*-hexane oxidation to alkanols, aldehydes, and ketones (7−8% terminal selectivity). The relative reactivity of primary and secondary C−H bonds in *n*-hexane was identical on both catalysts ($k_{prim}/k_{sec} = 0.10-0.11$) and similar to that predicted from relative C−H bond energies in *n*-hexane using Evans−Polanyi relations. Spatial constraints within MnAPO-18 did not lead to any preference for terminal oxidation or to hexanoic acid as the main product, in contradiction with previous reports on materials with identical structure. The lack of specific regioselectivity on MnAPO-18 is not unexpected, in view of its large intracrystalline cages, of the accepted involvement of ROOH intermediates, and of the lack of diffusional constraints on the rates of *n*-hexane oxidation on MnAPO-18 catalysts.

Introduction

The oxidation of alkanes to more valuable products has been extensively studied.[1,2] In most instances, the strength of the C−H bonds involved controls the rate and selectivity of oxidation turnovers.[3,4] As a result, preferential oxidation at specific C−H bonds, except as dictated by their relative bond strengths, remains a formidable challenge. C−H bonds at terminal positions in *n*-alkanes are ∼13 kJ/mol stronger than secondary C−H bonds[5] (e.g., 410 vs 397 kJ/mol for propane); thus, terminal oxidation selectivities are typically below 10% in C_{10-} alkanes, unless spatial constraints, imposed by the H-abstractor or by the structure of the voids around active sites, favor terminal attachment or inhibit access to secondary or tertiary carbons. Severe steric constraints around catalytic sites have led to modest terminal selectivities in homogeneous organometallic porphyrin complexes, as well as in heterogeneous catalysts. For homogeneous Mn-tetraphenylporphyrins, 26% terminal selectivity for *n*-octane oxidation was observed using iodosobenzene as the oxidant,[6] corresponding to $k_{prim}/k_{sec} = 0.70$ (defined as the ratio of primary to secondary products normalized by the number of each type of C−H bonds). For heterogeneous catalysts, 21% ($k_{prim}/k_{sec} = 0.54$) for *n*-octane on Fe/Pd/zeolite A,[7] 45% ($k_{prim}/k_{sec} = 1.6$) for *n*-octane on Fe−ZSM-5,[8] and 32% ($k_{prim}/k_{sec} = 0.63$) for *n*-hexane on VS-2[9] with added or in situ generated H_2O_2 have been observed. *n*-Octane oxidation products were removed from zeolite A only by dissolving the zeolites after the reaction.[7] Zeolite-based catalysts with 10-membered rings and ∼5 Å channels also showed some regioselectivity in alkane chlorination.[10−13] Terminal selectivities as high as 65.5% ($k_{prim}/k_{sec} = 2.5$) for *n*-hexane were recently reported for *n*-alkane oxidation (with O_2) on MnAPO-18 and CoAPO-18 catalysts containing small 8-member ring (3.8 Å) windows connecting large pear-shaped cages (7−12 Å).[14−20] These selectivities are unprecedented; they also are noteworthy for their almost exclusive preference for alkanoic acids among terminal oxidation products. Several studies have speculated about the practical and mechanistic implications of such terminal selectivities,[21,22] but there are no confirming reports, and one study presents evidence against any specific regioselectivity during *n*-octane oxidation on CoAPO-18.[23]

We recently have examined the structure and redox properties of Me-sites (Me = Mn, Co) in MeAPO-5 and MeAPO-18 catalysts[24] and the mechanism of cycloalkane oxidation.[25] Here, we examine regiospecificity and reactant selectivity in alkane oxidation in the context of these mechanisms and site requirements to assess the role of spatial constraints on regioselectivity and on the relative rate of oxidation for hydrocarbon molecules of varying size.

Experimental Methods

The experimental details for the synthesis, characterization, and rate measurements have been reported elsewhere;[24,25] we include here only details of direct relevance to the present study. MnAPO-5[26] and MnAPO-18[27] were prepared using reported

* To whom correspondence should be addressed. E-mail: iglesia@berkeley.edu. Tel: (510)-642-9673. Fax: (510)-642-4778.
[†] University of California at Berkeley.
[‡] ExxonMobil Research and Engineering Co.

10.1021/jp062869v CCC: $37.00
Published on Web 12/22/2006

TABLE 1: Redox Fractions (Mn_{redox}/Mn_{total}) in MnAPO-18 and MnAPO-5 Materials Obtained from H_2−TPR, EXAFS and EPR

			redox fraction		
catalyst	reference	Mn/P	H_2-TPR	EXAFS	EPR
MnAPO−18	[24]	0.050	0.86		
MnAPO−18	[29]	0.08		1.00	
MnAPO−18	[31]	0.005		1.00	0.80
MnAPO−5	[24]	0.055	0.62		
MnAPO−5	[29]	0.08		0.63	
MnAPO−5	[31]	0.005		0.58	0.50

methods. X-ray diffraction patterns and micropore volumes determined by *n*-hexane adsorption at 423 K were identical to those reported in the original literature and were consistent with known AlPO-5 and AlPO-18 crystal structures. X-ray diffraction data (Figure 1 in the Supporting Information) for MnAPO-18 detected only AlPO-18, without any evidence for AlPO-5 or other crystalline structures.

The redox properties of Mn cations, measured from reversible changes in the oxidation state during treatments in H_2 and O_2, confirmed the presence of most Mn-sites at framework positions in which Mn centers can undergo $Mn^{2+}-Mn^{3+}$ redox cycles;[24] MeAPO-18 had a higher fraction of the Mn in redox-active structures relative to MeAPO−5, as also reported in comparative studies.[28,29]

The catalytic oxidation of *n*-hexane (25 cm^3; 99.5% purity; Fluka, <0.1% impurities other than methylpentanes and dimethylbutanes) was carried out in a shielded, stirred high-pressure glass reactor (Andrews Glass; 100 cm^3) at 403 K (0.2 g of catalyst; 0.55 MPa O_2, Airgas, UHP; 200−300 rpm). These *n*-hexane volume/catalyst ratios are identical to those used previously.[14] O_2 was periodically dosed during reaction to maintain a constant O_2 pressure (0.55 ± 0.01 MPa; total pressure 0.75 MPa) and to ensure rigorous analysis of the dynamics of product formation. Liquid samples (∼0.5 cm^3) were extracted periodically (every ∼1 h; at least eight samples per experiment) and reactant and product concentrations were measured using an internal standard (0.2 cm^3 *o*-dichlorobenzene) by gas chromatography (Hewlett-Packard 5890) with a DB-wax column (60 m in length, 0.32 mm in diameter and 0.5 μm film thickness) and a flame ionization detector (FID). Alkanoic acids (C_2-C_6 acids), formed via oxidation of hexanols, hexanal, and hexanones, were measured directly using the same chromatographic protocols without the intervening derivatization previously used.[14] Formic acid (C_1 acid) was not detected by this analysis protocol because of its low flame ionization sensitivity. A typical chromatogram of the reaction products is shown (Figure 2 in the Supporting Information). Reaction rates are reported on the basis of *n*-hexane (C_6) converted to each product, noting that two shorter acids (C_1-C_5 acids) form when a C−C bond within oxidation products (ketones and alcohols) is cleaved.

The concentration of hexyl hydroperoxide isomers was measured by reacting them with triphenylphosphine (Sigma-Aldrich) to form the corresponding hexanol isomers and measuring the hexanol concentrations before and after derivatization with triphenylphosphine.[30]

Results and Discussion

Characterization of MnAPO-18 and MnAPO-5 Materials. First, we show that MnAPO-18 and MnAPO-5 materials used here (and described previously)[24] are structurally identical to those used in comparative studies.[14] The fraction of the Mn atoms present as redox-active sites (Mn_{redox}/Mn_{total}) was determined by H_2-O_2 cycles and UV−visible spectroscopy[24] and compared with estimates from X-ray absorption fine structure (EXAFS) data[14,29] (Table 1). These data also are compared with recent electron paramagnetic resonance (EPR) and EXAFS studies[31] on similar samples (Table 1). The fraction of the Mn atoms present as redox-active cations was 0.50−0.63 for MnAPO-5 using these methods and 0.80−0.86 for MnAPO-18 using H_2-O_2 cycles and EPR. A previous study assumed that the (Mn_{redox}/Mn_{total}) ratio was unity for MnAPO-18, because it gave the shortest EXAFS Mn−O and was considered to contain the highest Mn^{3+} fraction among MnAPO materials;[29] the redox fractions were reported relative to MnAPO-18 for the other samples, as also done previously for CoAPO samples.[28] While there is no independent evidence for the assumed redox fraction of unity (from EXAFS) for MnAPO-18, H_2−TPR and EPR methods provide direct and accurate absolute values of the redox-active fractions based on measured amounts of H_2 consumption[24] or residual Mn^{2+} after O_2 treatment, respectively;[31] the methods are better suited for detecting minority fractions of permanently divalent species than X-ray absorption spectra. We conclude from these data that the catalysts used here are identical in structure and redox properties to those in earlier studies[14,28,29] and in recent comparative studies,[31] a conclusion expected from the identical protocols used to prepare these samples.

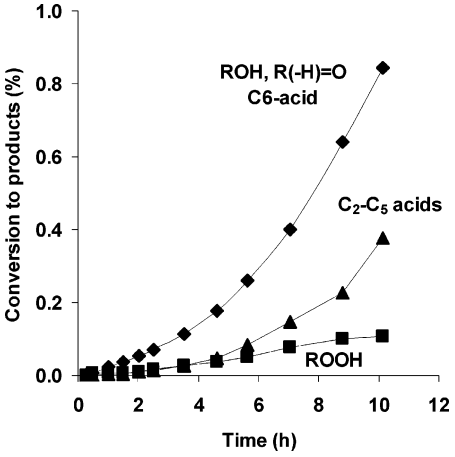

Figure 1. *n*-Hexane conversion to products on MnAPO-18 [403 K, 0.55 MPa O_2, 0.2 g of MnAPO-18, 25 mL of *n*-hexane].

***n*-Hexane and Cyclohexane Oxidation Rates on MnAPO-18 and MnAPO-5.** The effects of the diameter and C−H bond strengths in molecules and of the spatial constraints imposed by AlPO channels on alkane oxidation rates and regioselectivity were examined on these MnAPO catalysts. Specifically, we report here oxidation reactions of cyclohexane (kinetic diameter 6.0 Å) and *n*-hexane (4.3 Å)[32] on MnAPO-5 (7.3 Å straight channels) and MnAPO-18 (3.8 Å windows connecting pear-shaped 7 × 12 Å cages). Rate constants are reported per active Mn_{redox} site for the alkyl hydroperoxide (ROOH) decomposition step, previously shown to be the sole kinetically-relevant step in cyclohexane oxidation catalyzed by MnAPO-5 materials.[25] The demonstrated involvement of ROOH in kinetically-relevant steps requires that its concentration be measured concurrently with those of the reaction products for rigorous kinetic comparisons among catalysts; yet, ROOH concentrations are not often measured and their decomposition rate constants have rarely been reported in previous studies.

The conversion of *n*-hexane into various oxidation products (ROOH, alcohols (ROH), ketones/aldehydes (R(−H)═O) and acids) on MnAPO-18 is shown in Figure 1 as a function of time. As in cyclohexane oxidation,[25] ROOH (1-, 2- and 3-hexyl

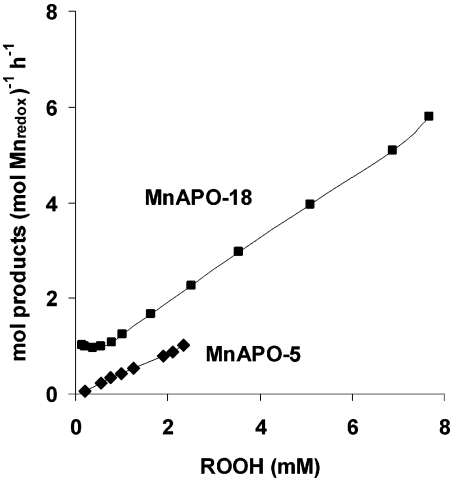

Figure 2. *n*-Hexyl hydroperoxide decomposition rate per Mn_{redox} vs lumped [ROOH] for *n*-hexane oxidation on MnAPO-18 and MnAPO-5. ROOH are 1-, 2-, and 3-hexyl hydroperoxides and alcohols, ketones, aldehydes, and acids are the main products that form from the hydroperoxides [403 K, 0.55 MPa O_2, 0.2 g of catalyst, 25 mL of *n*-hexane].

TABLE 2: ROOH Decomposition Rate Constants for *n*-Hexane and Cyclohexane Oxidation Normalized Per Mn_{redox} and [ROOH] in MnAPO-5 and MnAPO-18

	(mol R(−H)═O + ROH) $(Mn_{redox})^{-1}$ (mM ROOH)$^{-1}$ h^{-1}	
catalyst	*n*-hexane	cyclohexane
MnAPO−18	0.38	0.10
MnAPO−5	0.31	0.46

hydroperoxides) decomposition rates into ROH, R(−H)═O, and acids were measured as a function of [ROOH] concentration (Figure 2). ROOH decomposition rates (per Mn_{redox}) are proportional to ROOH, as shown previously for cyclohexane,[25] except in the initial stages during which active sites reach their steady-state, as discussed below. Turnover rates for *n*-hexyl hydroperoxide decomposition were essentially identical on MnAPO-5 and MnAPO-18 (Table 2), indicating that redox-active sites, but not permanently divalent sites, are involved in kinetically-relevant ROOH decomposition steps. These data also show that the intrinsic reactivity of Mn_{redox} sites are similar on these two catalysts and that such sites are accessible without significant transport restrictions within both AlPO channel structures. These observations indicate that measured rates are kinetic in nature, uncorrupted by transport restrictions, and unaffected by spatial constraints, which would have been much more severe through the smaller windows in MnAPO-18 (3.8 Å) than for the larger channels in MnAPO-5 (7.3 Å). The rapid transport of *n*-hexane into MnAPO-18 crystallites was confirmed by *n*-hexane adsorption measurements for MnAPO-5 and MnAPO-18 (Figure 3), which reached saturation levels in a short time (<0.1 h). Typical reaction times are ∼1.0 h, based on converting 1/e of the intracrystalline *n*-hexane (8.3 *n*-hexane/Mn_{redox}) at typical turnover rates (30 product molecules/Mn_{redox} in 10 h); thus, *n*-hexane molecules diffuse much more rapidly within intracrystalline voids than they react within such voids in MnAPO-18.

Alkane Oxidation Pathways on MnAPO Materials. Alkane oxidation on homogeneous Co- and Mn-based catalysts has been proposed to occur via Haber−Weiss mechanisms involving free radicals.[1,2] We have previously reported cyclohexane oxidation kinetic and isotopic studies on MnAPO-5 and have suggested an alternate mechanism, which avoids free radical and charged

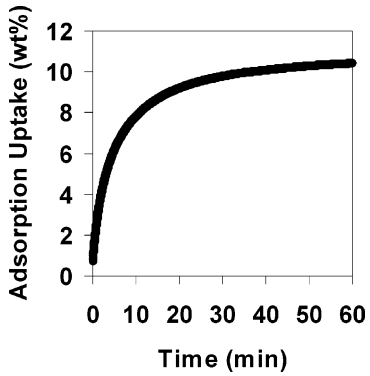

Figure 3. *n*-Hexane adsorption uptake at 298 K for MnAPO-18.

SCHEME 1: Free Radical-Based Alkane (RH) Oxidation Pathways[1,21]

Classical Initiation Steps[1]

i. $Me^{2+} + ROOH \rightarrow Me^{3+} + RO^{\cdot} + OH^{-}$

ii. $Me^{3+} + ROOH \rightarrow Me^{2+} + ROO^{\cdot} + H^{+}$

Alternate Initiation Steps

i-b. $[Me^{2+}\text{-}O\text{-}H] + ROOH \rightarrow [Me^{3+}\text{-}O] + RO^{\cdot} + H_2O$

ii-b. $[Me^{3+}\text{-}O] + ROOH \rightarrow [Me^{2+}\text{-}O\text{-}H] + ROO^{\cdot}$

Propagation

iii. $RO^{\cdot} + RH \rightarrow ROH + R^{\cdot}$

iv. $R^{\cdot} + O_2 \rightarrow ROO^{\cdot}$

v. $ROO^{\cdot} + RH \rightarrow ROOH + R^{\cdot}$

Termination

vi. $ROO^{\cdot} + ROO^{\cdot} \rightarrow ROH + R(-H)=O + O_2$

If steady-state is assumed for the radical concentrations, the ROOH decomposition stoichiometry of steps (i)-(iv) and (vi) is:

vii. $2\ ROOH + RH \rightarrow 2\ ROH + R(-H)=O + H_2O$,

whereas the ROOH formation stoichiometry from steps (iv) and (v) is:

viii. $RH + O_2 \rightarrow ROOH.$

The classical initiation steps (i) and (ii) involving reactions of free H^+ and OH^- ions can be replaced with corresponding reactions of bound intermediates (steps (i-b) and (ii-b)).

intermediates in the liquid phase and replaces them with bound radical-like species.[25] *n*-Hexane oxidation kinetic equations are identical to those for cyclohexane; thus, we adapt here these heterogeneous pathways to examine steps in which regioselectivity may be influenced for *n*-hexane reactants. We compare a Haber−Weiss mechanism in two slightly different forms in Scheme 1 with a heterogeneous version in Scheme 2[25] that shares several common intermediates (e.g., ROO, RO, and R), albeit as bound species. Steps (i)−(vi) in Scheme 1[1,21] have both free radicals and ionic species with H_2O forming from free OH^- and H^+ ions. Instead, we propose the initiation steps (i-b) and (ii-b) in Scheme 1 to avoid the formation of free ions, thus forming water via the bound H-intermediates that are prevalent for solid acid catalysts. The removal and formation of bound H-intermediates in steps (i-b) and (ii-b) is reasonable for these heterogeneous MnAPO catalysts in which redox sites are able to reversibly form and remove H that is associated with bound O−H groups.[24] The propagation and termination steps (iii)−(vi) are the same for the two different initiation pathways in Scheme 1.

In an alternate mechanism[25] involving bound intermediates (Scheme 2, also shown in Figure 4), step (1) in Scheme 2 is essentially the same as step (i-b) in Scheme 1, except that RO

SCHEME 2: Proposed Elementary Steps for Alkane (RH) Oxidation

1.	H*	+ ROOH	→	RO*	+ H_2O
2.	RO*	+ R'H	→	R'*	+ ROH
3.	R'*	+ O_2	→	R'OO*	
4.	R'OO*		→	OH*	+ R'(-H)=O
5.	OH*	+ RH	→	H*	+ ROH
6.	R'OO*	+ R'H	→	R'*	+ R'OOH

The stoichiometry of the ROOH decomposition cycle of steps (1)-(5) is:

7. ROOH + 2 RH + O_2 → 2 ROH + R(-H)=O + H_2O ,

whereas the ROOH formation stoichiometry from steps (3) and (6) is:

8. RH + O_2 → ROOH.

A cyclic representation of this scheme is shown in Figure 4, in which the structures of H*, RO*, R'*, R'OO* and OH* are shown in more detail. The R and R' notations are used to denote distinct alkyl groups in bimolecular steps.

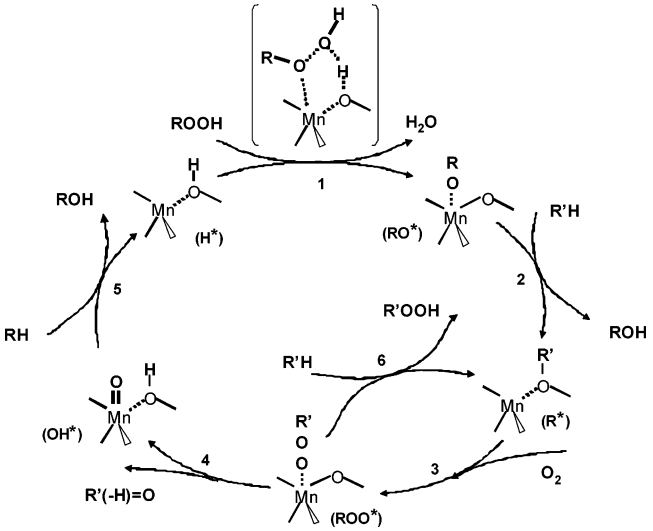

Figure 4. Cyclic scheme for alkane oxidation on MnAPO materials (adapted from the steps in Scheme 2).

species remain bound. Bound RO intermediates then react with an alkane, and the subsequent reaction of the formed R intermediate with O_2 occurs both in steps (2) and (3) of Scheme 2 and in steps (iii) and (iv) of Scheme 1, the only difference being that R and ROO are bound species in Scheme 2. Propagation steps that form ROOH have the same stoichiometry in steps (6) and (3) in Scheme 2 as in steps (iv) and (v) in Scheme 1. The two mechanisms differ, however, in the steps leading to R(−H)═O. In Scheme 1, two ROO radicals recombine to form R(−H)═O, ROH, and O_2 in a concerted bimolecular termination step (step (vi)); in contrast, R(−H)═O and ROH form in sequential steps (4) and (5) in Scheme 2. In step (4), vicinal Mn−O species abstract a hydrogen atom from ROO* to form R(−H)═O. In the subsequent step (5), the Mn═O species in OH* formed in step (4) react with an alkane to form ROH in a similar fashion as that observed for oxidation reactions on porphyrin-based catalysts, for which a rebound-type mechanism has been proposed.[33]

An earlier study[21] suggested that the higher oxidation rates generally observed for tertiary vs primary and secondary alkanes was due to slower termination steps for the former, in which the R(−H)═O formation in step (vi) in Scheme 1 is not possible, leading to higher radical concentrations and more rapid oxidation rates. Our proposed steps in Scheme 2 can also explain this difference. For ROO* to react in step (4), it needs to be able to give up a hydrogen atom to form R(−H)═O, a reaction that primary and secondary ROO species can do, but tertiary ones cannot. Therefore, tertiary ROO* species would much rather react in step (6) than in step (4) leading to rapid build-up of tertiary hydroperoxides and high overall rates, similar to what is expected when step (v) is favored over step (vi) in Scheme 1. Thus, the inhibited R(−H)═O formation pathways compared to those for ROOH formation for tertiary ROO-species are a shared feature of Schemes 1 and 2 and explain why tertiary alkanes react more rapidly than primary and secondary ones.

The stoichiometries of Schemes 1 and 2 are nearly identical, and we propose Scheme 2 as an alternative mechanism to the one usually invoked to explain alkane autoxidation with O_2 as the oxidant (Scheme 1).[1] The cycle in Scheme 2 and Figure 4 leads to the measured product stoichiometry via steps that mimic those proposed for free radicals but does not require solvation by the liquid, which is a process that is unlikely to occur with the small number of molecules within intracrystalline voids, or termination steps involving bimolecular reactions of bulky free radicals, present at very low concentrations, during each catalytic turnover. The first-order ROOH dependence indicates that step (1) is the kinetically-relevant step; the bimolecular ROO reaction in step (vi) of Scheme 1 would lead to a second-order ROOH dependence for catalytic reactions, which we observe only for noncatalytic alkane oxidation, in which the bimolecular termination step is kinetically-relevant.[34]

Except for the most abundant divalent H* intermediate, we have no direct kinetic or spectroscopic evidence for the intermediates in Scheme 2, because their reactions occur after the kinetically-relevant ROOH activation steps (step (1) in Scheme 2). Metal−OOR intermediates, however, have been proposed for alkane oxidation catalyzed by homogeneous Co complexes,[35,36] and metal−oxo intermediates are common for porphyrin catalysts.[33] We can assign formal oxidation states to the different bound intermediates in Scheme 2 (Figure 4) based on the assumptions that RO* and ROO* intermediates are radical-like (RO and ROO are neutral ligands) and OH* metal−oxo-like. Also, when H or R become bound to a neighboring O in H* and R*, this O-based ligand becomes formally neutral instead of negatively charged, resulting in a net one-electron reduction of Mn centers. In Figure 4, we denote interactions of neutral and anionic ligands with Mn by dotted and solid lines, respectively; the dotted lines do not involve formal electron transfer between Mn and the ligand. The real charge on the Mn-center depends on whether the reaction intermediates are partially charged and the extent to which the binding between Mn and neighboring framework oxygen atoms changes as different intermediates are bound. From UV−vis spectroscopy, the resting state and the most abundant intermediate is the divalent form of the Mn redox sites (H*),[25] and as H* reacts with ROOH in step (1) to remove H from the neighboring O and binds the neutral RO, its oxidation state increases to Mn^{3+}. Mn^{3+} reduces to Mn^{2+} as R binds to a vicinal oxygen atom (R*) in step (2) and then reoxidizes to Mn^{3+} when ROO* forms in step (3). In step (4), ROO* reacts to form a bound metal−oxo species and a bound H in the OH* species; we assign a formal oxidation state of Mn^{4+}═O^{2-} to the metal−oxo species. The metal−oxo species in OH* then reacts with RH to return to the resting divalent state of H* in step (5). Regardless of the exact nature of the reactive intermediates, Mn goes through different oxidation states as H is added and removed in the cycle, requiring redox-active Mn-centers, in agreement with our correlation of Mn redox fraction and ROOH decomposition activity for a series of MnAPO-5 materials.[25] The ability of neighboring oxygen atoms to add and remove H during H_2−O_2 cycles,[24] as well as during ROOH decomposition and

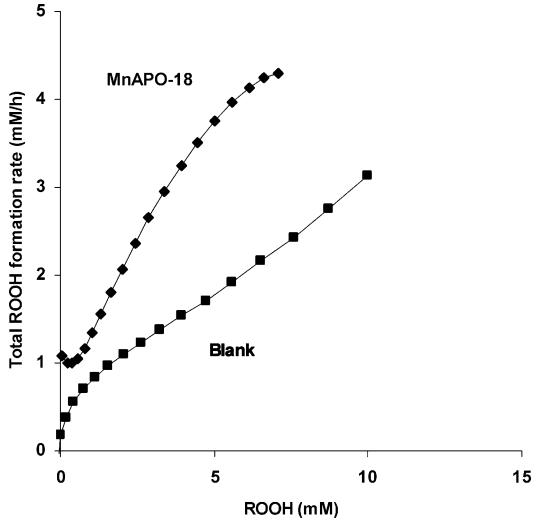

Figure 5. Total ROOH formation rates (net ROOH measured + ROOH being decomposed) during *n*-hexane oxidation in the presence and absence of MnAPO-18 [403 K, 0.55 MPa O_2, 0.2 g of MnAPO-18 or no catalyst, 25 mL of *n*-hexane].

formation cycles (Scheme 2),[25] is a key feature of the activity of isolated Mn redox sites in these MnAPO materials and may be important for alkane oxidation on homogeneous Mn and Co catalysts as well. We discuss oxidation rates and regioselectivity below with reference to the pathways depicted schematically in Scheme 2 and Figure 4.

Competing Pathways for ROOH Formation and Decomposition for *n*-Hexane and Cyclohexane Oxidation on MnAPO-18 and MnAPO-5. As in the case of ROOH decomposition, ROOH formation rates must be measured as a function of ROOH concentration, because it can form via heterogeneous and noncatalytic pathways, which depend differently on ROOH concentration and which would be affected differently by spatial constraints. Noncatalytic pathways have been widely discussed[1,2] and their mechanistic details recently reexamined.[37] Noncatalytic ROOH formation outside AlPO channels lead to nonselective oxygen insertion along the alkane chain and to the dilution of any prevalent effects of spatial constraints on regioselectivity. Catalytic and noncatalytic pathways can be distinguished from the different rate dependence for ROOH formation as a function of ROOH concentration in the presence and absence of a catalyst. Here, we compare total ROOH formation rates (the sum of the measured net ROOH formation rate and the rate of ROOH decomposition to form products; Scheme 2) for MnAPO-18 and for noncatalytic autoxidation reactions. ROOH consumption rates are given by the rate of ROH + R(−H)═O formation (divided by 3, from the stoichiometry of steps (1)−(5) in Scheme 2). Noncatalytic hexyl hydroperoxide formation rates are lower than catalytic rates on MnAPO-18 at all ROOH concentrations (Figure 5), indicating that active sites in MnAPO-18 form a significant fraction of the ROOH molecules detected either directly or from their products. The relative rates of catalytic and noncatalytic ROOH formation rates, however, vary as [ROOH] concentrations increase with increasing reaction time. At the low [ROOH] concentrations initially prevalent, heterogeneous ROOH formation rates have a nonzero intercept (discussed in detail below), while noncatalytic oxidation rates extrapolate to zero. Noncatalytic ROOH formation rates increase faster than linearly with [ROOH] concentration, while catalytic ones show a weaker than linear [ROOH] dependence (Figure 5). Noncatalytic ROOH formation rates approach catalytic rates on MnAPO-18 and ultimately surpass them as the ROOH concentration increases, making it difficult to preserve any regiospecificity induced by spatial constraints as alkane conversion increases. Any regiospecificity caused by a catalyst would be most apparent at low conversions, at which catalytic ROOH formation pathways predominate.

The similar *n*-hexane oxidation rates (per Mn_{redox}) on MnAPO-18 and MnAPO-5 indicate that their different rates for oxidation of larger molecules, such as cyclohexane, reflect reactant selectivity effects imposed by channel size effects on the diffusion of molecules within small windows in MnAPO-18. Cyclohexyl hydroperoxide decomposition turnover rates were 4.6 times smaller on MnAPO-18 than on MnAPO-5 (Table 2). These data suggest that intrachannel redox-active sites in MnAPO-18 are inaccessible to cyclohexane; they also confirm that redox-active sites reside predominantly within such channels. The rate of cyclohexyl hydroperoxide formation on MnAPO-18 is similar to that measured during noncatalytic cyclohexane oxidation; cyclohexyl hydroperoxide decomposition rates are also very similar (∼1.5 larger) on MnAPO-18 and for homogeneous reactions. Thus, cyclohexyl hydroperoxide formation with MnAPO-18 catalysts occurs predominantly via homogeneous pathways, while its decomposition occurs via parallel homogeneous and catalytic pathways; the latter apparently occurs on external surfaces of MnAPO-18 crystallites because cyclohexane (6.0 Å kinetic diameter)[32] cannot diffuse within the small windows in AlPO-18 (3.8 Å). We conclude that MnAPO-18 is able to select reactants based on their relative size by restricting their access to intrachannel Mn_{redox} sites required for kinetically-relevant ROOH decomposition steps.

Regioselectivities for O-Attachment during *n*-Hexane Oxidation on MnAPO-18 and MnAPO-5. The role of channel geometry on *n*-hexane oxidation regioselectivity was also examined on MnAPO-5 and MnAPO-18 to assess how spatial constraints may influence the activation of specific C−H bonds in *n*-alkanes. Table 3 shows *n*-hexane oxidation conversion and selectivity data on MeAPO samples used here, together with data reported previously,[14] at similar *n*-hexane/catalyst ratios and 373 K. The conversion of *n*-hexane on MnAPO-18 is ∼2.8−3.0 higher than on MeAPO-5 in both this study (at 403 K) and in the earlier study (at 373 K),[14] even though the rate constants for ROOH decomposition are essentially identical in the two catalysts (Table 2). The higher conversion measured on MnAPO-18 (Table 3) reflects the higher fraction of redox sites on MnAPO-18 compared with MnAPO-5 (Table 1), as well as the higher ROOH concentrations prevalent on MnAPO-18 relative to MnAPO-5; the latter appears to reflect a slightly higher ROOH formation on MnAPO-18. These comparative rate data on MnAPO-18 and MnAPO-5 indicate that any MnAPO-5 impurities in MnAPO-18 samples (undetectable by any of the methods used) could not influence the rates and selectivities reported here on MnAPO-18.

MnAPO-5 and MnAPO-18 catalysts gave identical terminal selectivities (6−8%; k_{prim}/k_{sec} = 0.09−0.12), which resemble values measured without a catalyst and agree with estimates from Evans−Polanyi free energy relations (shown below) obtained using known C−H bond energies. They also resemble terminal selectivities reported for *n*-octane oxidation on CoAPO-18 catalysts,[23] but differ markedly from values reported on MnAPO-18 (65.5%; k_{prim}/k_{sec} = 2.5) and CoAPO-18 (61.3%; k_{prim}/k_{sec} = 2.1)[14] catalysts with identical structure and composition to those used here. Terminal selectivities are similar for MnAPO-18 and for noncatalytic reactions even at low conversions, which favor products of catalytic pathways, indicating that heterogeneous ROOH formation pathways on MnAPO-18

TABLE 3: Conversion and C_6-Based Selectivity (Each *n*-Hexane Gives Two Short Acids) for *n*-Hexane Oxidation on MeAPO Materials[a]

		selectivity [%]										
catalyst	conv [%]	R_1OOH	R_1OH	$R_1{=}O$	C_6- acid	R_2OOH	R_2OH	$R_2{=}O$	R_3OOH	R_3OH	$R_3{=}O$	C_2-C_5 acids
					previous study[14]							
CoAPO−5	2.4		1.3	4.1	3.2		3.2	6.0		41.0	30.4	
CoAPO−18	7.2		4.5	3.3	53.5	-	13.9	22.2				
MnAPO−18	8.7		9.9	12.5	43.1		8.4	23.3				
					this study							
MnAPO−5	0.5	1.1	1.8	1.1	1.2	12.4	12.2	12	9.3	16.2	13.5	19.1
MnAPO−18	1.4	0.38	1.75	0.22	1.79	4.3	12.3	12.9	2.9	15.6	14.5	33.3

[a] Conditions of both studies. Previous study:[14] 373 K, 50 g of *n*-hexane, 0.5 g of catalyst, 1.5 MPa air at 298 K (0.3 MPa O_2), 24 h. This study: 403 K, 16.5 g of *n*-hexane, 0.2 g of catalyst, 0.55 MPa O_2 and 0.75 total pressure at 403 K, 10 h.

do not lead to enhanced terminal selectivity. The low terminal selectivity measured on MnAPO-18 is not unexpected in view of the large internal cages, within which spheres as large as 7.27 Å can be inscribed,[38] and of the high diffusivity of *n*-hexane in MnAPO-18 (Figure 3). One such inscribed sphere has a volume of 201 $Å^3$, while one *n*-hexane molecule has a volume of 77 $Å^3$ (from its liquid density at 298 K). The presence of several *n*-hexane (and/or ROOH) molecules within each cage and their high intercage transfer rates suggest that the selectivity of heterogeneous oxygen attachment may be controlled by the rattling of one or several molecules within a cage rather than by any collimation effects of small windows on *n*-alkane molecules approaching active sites. Thus, we conclude that MnAPO-18 windows affect neither the rate nor the selectivity of O-attachment during oxidation of *n*-hexane with O_2.

Oxidation rates show an initial induction period (Figure 5) as Mn^{3+} cations, present on air-treated MnAPO catalysts, and also activate C−H bonds stoichiometrically and lead to an initial rapid increase in ROOH concentration, as shown also for cyclohexane oxidation on MnAPO-5.[25] ROOH formation rates extrapolate to nonzero values at zero ROOH concentrations and increase monotonically with increasing ROOH concentration above ~0.5 mM ROOH (corresponding to ~2 turnovers per Mn_{redox}). Thus, these first few turnovers within the induction period can be preferentially influenced by the presence of Mn^{3+}, but after [ROOH] increases, the catalyst reaches its steady-state Mn^{2+} form, as in the case of cyclohexane oxidation[25] and as reported earlier for *n*-hexane oxidation.[14] For the >30 turnovers in the present study and the >150 turnovers in the earlier study,[14] the relevant C−H bond activation processes occur at the steady-state via steps (2), (5), and (6) in Figure 4, as discussed in the last section of this article. Any initial collimation or preferred docking of *n*-alkanes via an end-on approach of terminal carbon atoms to Me^{3+} centers within large cages in MeAPO-18[14] would be relevant only during the first few turnovers and essentially undetectable after 30−150 turnovers. As mentioned above, terminal selectivities during the induction period, in which stoichiometric reduction of Mn^{3+} is involved in C−H activation, were slightly lower (~6%) than at steady-state (~7%) (Figure 6). These data suggest that these stoichiometric interactions, as well as the pathways in Scheme 2, prevalent at the steady-state, occur without any regiospecificity on MnAPO-18. Abstracting species in heterogeneous and in noncatalytic pathways consist primarily of ROO and RO species, whether free or adsorbed, and abstract hydrogen atoms with similar specificity and dependence on the strength of the C−H being activated.

In previous studies, alkanoic acids were predominantly responsible for the unprecedented terminal selectivity reported on MeAPO-18[14] (up to 53.5% of total products, Table 3; also see Figure 2a and Table 1 in ref 14). We also have detected significant amounts of alkanoic acids during *n*-hexane oxidation

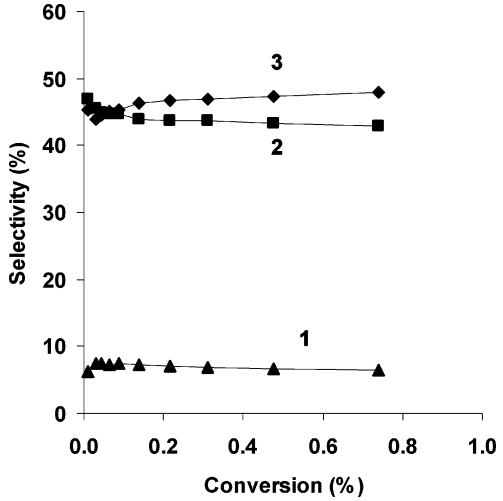

Figure 6. Selectivities to 1-, 2-, and 3-oxygenates of function of conversion [403 K, 0.55 MPa O_2, 0.2 g of MnAPO-18, 25 mL of *n*-hexane].

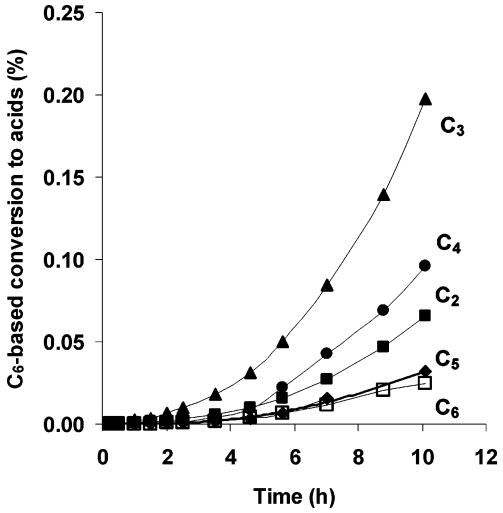

Figure 7. C_6-based conversion to different acid products (C_2−C_6 acids) during *n*-hexane oxidation on MnAPO-18 [403 K, 0.55 MPa O_2, 0.2 g of MnAPO-18, 25 mL of *n*-hexane].

on MnAPO catalysts but with the expected prevalence of smaller acids, formed via sequential oxidation of hexanones and of 2- and 3-hexanols. Our direct analysis of the acids formed detected 1−2% hexanoic acid selectivity at 0.5−1.5% *n*-hexane conversion on MnAPO-5 and MnAPO-18 (Table 3). The predominant acid products were shorter C_2−C_5 chains, which became more prevalent as the *n*-hexane conversion increased (Figure 7 and Table 3); on a C_6-basis, these short acids (formed via C−C bond cleavage) are present at levels 12−15 times higher than for

hexanoic acid, consistent with the lack of regiospecificity for oxygen insertion by these materials. The significant levels of shorter acids in the present study are consistent with earlier studies in which homogeneous Co and Mn salts[39] and $RhCl_3$ complexes[40] were shown to be effective catalysts for C−C bond cleavage in ketones and internal alkanols. The facile degradation of the carbon backbone to form C_4- and C_2-acids also is apparent from previous reports of *n*-hexane oxidation on CoAPO-5[41] in which the most abundant initial oxidation products were 2-hexanol and 2-hexanone, as in the present study. Secondary oxidation of ketones requires C−C bond cleavage, as in the synthesis of adipic acid from cyclohexanone[1,42] but with the formation of two smaller acids instead of the diacid in the case of the acyclic alkanes. These shorter acids contain O-atoms at terminal positions as a result of C−C bond cleavage, but they do not reflect oxidation at terminal carbons in primary or secondary reactions. Small-window MnAPO-18 (3.8 × 3.8 Å) gave higher selectivities to C_2−C_5 acids than MnAPO-5 (7.3 × 7.3 Å) (Table 3), as also shown in a recent study,[23] because secondary reactions become more prevalent at the higher conversion levels typically achieved on MeAPO-18, which contains a larger fraction of redox-active sites than MnAPO-5. If all acids were defined as terminal oxidation products, the apparent terminal selectivity on MnAPO-18 would be 55%, a value coincidentally similar to the unprecedented and unconfirmed terminal selectivities reported in a comparative study (∼65%).[14]

The selectivity to all acids increased with contact time (Figure 7) and shorter acids were the predominant products because of preferential oxidation at nonterminal carbons in both the initial C−H activation and the sequential oxidation of its initial products. The assumption that acids form via sequential oxidation of hexanal or hexanones led us to include acids with the latter in reporting ROH/R(−H)═O ratios. The resulting ROH/[R(−H)═O + C_6-acid] ratios were similar (1.0−1.3) for products resulting from oxidation at the 1-, 2-, and 3-positions (Figure 8a), whereas excluding hexanoic acid led to much higher ROH/R(−H)═O ratios, suggesting indeed that hexanoic acid is produced from secondary oxidation of hexanal.

In the case of cyclohexane oxidation on MnAPO-5,[25] initial ROH/R(−H)═O ratios (1.7−2.5) were consistent with the value of 2 expected from Scheme 2, whereas ROH/[R(−H)═O + C_6-acid] ratios were smaller (1.0−1.3) for *n*-hexane oxidation (Figure 8a). The similar first-order ROOH decomposition kinetics for *n*-hexane and cyclohexane oxidation would suggest that Scheme 2 is prevalent for both *n*-hexane and cyclohexane. Some details, however, must be reconsidered in light of these different ROH/[R(−H)═O + C_6-acid] ratios. Rapid secondary oxidation of ROH would decrease ROH/[R(−H)═O + C_6-acid] ratios. This possibility was tested by adding a secondary alcohol (2-butanol) to scavenge reactive species responsible for rapid hydrogen abstraction from hexanols. The presence of 2-butanol during *n*-hexane oxidation on MnAPO-18 led to initial ROH/[R(−H)═O + C_6-acid] ratios of 1.9 ± 0.2 (Figure 8b); these values are much larger than those measured in the absence of 2-butanol and are similar to the value of 2 expected from the steps in Scheme 2. 2-Butanol reacts with H-abstracting intermediates, such as OH* in Step (5), as previously proposed for secondary cyclohexanol oxidation on MnAPO-5[25] thus preventing rapid dehydrogenation of the hexanol molecules formed within ROOH decomposition cycles. These data indicate that *n*-hexane and cyclohexane oxidation reactions indeed occur via elementary steps similar to those previously proposed for cyclohexane reactants.[25]

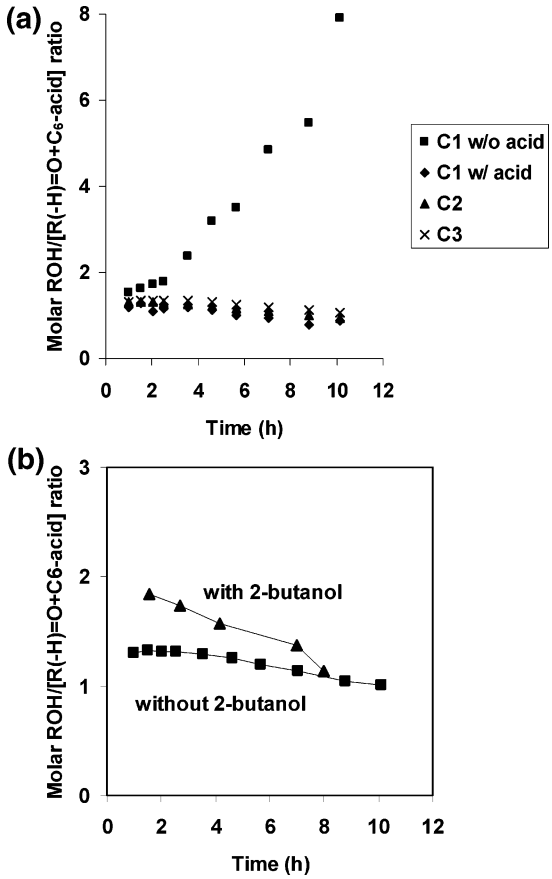

Figure 8. Ratios of alcohol to secondary oxidation products (ketones, aldehydes, and C_6-acid) (a) for each carbon-position during *n*-hexane oxidation on MnAPO-18. For C_1-oxygenates, both 1-hexanol/hexanal and 1-hexanol/(hexanal + hexanoic acid) are shown. (b) In total with and without 2-butanol addition [403 K, 0.55 MPa O_2, 0.2 g of MnAPO-18, 25 mL of *n*-hexane].

Oxidation turnover rates for *n*-hexane were lower than for cyclohexane on MnAPO-5 (at 403 K), a trend similar to that reported previously on CoAPO-5.[41] The energies for secondary C−H bonds in *n*-hexane and cyclohexane are nearly identical (397 kJ/mol);[5] cyclohexyl hydroperoxides form more rapidly than *n*-hexyl hydroperoxides because of the larger number of secondary C−H bonds (12 vs 8) and the weaker steric bulk around C−H bonds in chair conformations of cyclohexane. Cyclohexane conversions on MnAPO-5[25] were similar to those previously reported,[17] suggesting that catalysts and reactants were similar in the two studies. The earlier study, however, reported that oxidation rates were higher for *n*-hexane (at 373 K) than for cyclohexane (at 403 K) on MeAPO-5.[17] *n*-Hexane conversions (∼0.02−0.05% at 373 K) measured here on MnAPO-5 and MnAPO-18 were ∼100 times smaller than reported previously on MnAPO-18 (7.2%).[14] The similar rates for cyclohexane reactants in the two studies suggest that *n*-hexane reflect differences in the reactants themselves (e.g., promoting impurities, such as branched alkanes, alkenes, or peroxides); we cannot comment further, however, because reactant purity was not reported in the comparative study. Branched alkanes with weak tertiary C−H bonds, ubiquitous as impurities in *n*-hexane, can form tertiary alkyl hydroperoxides even during storage; these are effective initiators for autoxidation reactions.[25] Our experiments involved *n*-hexane of the highest available purity (Fluka, 99.5%, <0.5% branched hexanes), which was confirmed by gas chromatography. We also carried out two control experiments to examine possible effects of

TABLE 4: Experimental and Calculated Oxidation Rate Ratios Per C−H Bond for Primary and Secondary Bonds in *n*-Hexane (k_{prim}/k_{sec}) during *n*-Hexane Oxidation on MnAPO-18 and MnAPO-5

	terminal selectivity	*n*-hexane ($k_{prim}k_{sec}$)	
catalyst	(%)	exp	calc
MnAPO−18	8	0.11	0.15
MnAPO−5	7	0.10	0.15
MnAPO−18[14]	65	2.5	0.15

branched alkanes or their hydroperoxides by adding branched alkanes or *tert*-butyl hydroperoxide (TBHP) to *n*-hexane during oxidation reactions on MnAPO-18.

The addition of 2-methylpentane (3% mol) or methylcyclohexane (3% mol) to *n*-hexane oxidation on MnAPO-18 led to a slight increase in oxidation rates (0.08% vs 0.05% after 8 h at 373 K). TBHP (0.4% mol) markedly increased oxidation rates (0.70% after 8 h at 373 K), but these remained 10 times smaller than in the previous study.[14] As for TBHP addition to cyclohexane oxidation,[25] ROOH formation rates were increased when TBHP was used for *n*-hexane oxidation, whereas ROOH decomposition rates were essentially unaffected by the presence of TBHP. Terminal selectivities were unchanged by the presence of branched alkanes or TBHP (5−7%, $k_{prim}/k_{sec} = 0.07-0.10$), indicating that regioselectivity was unaffected by temperature (373 K vs 403 K) or by reactive impurities in *n*-hexane.

Ratios of C−H Bond Activation Rates and Evans−Polanyi Free Energy Relations. We examine next the effects of C−H bond energies on reactivity and on oxidation regioselectivity in the context of Evans−Polanyi relations[43,44] and the oxidation pathways in Scheme 2. Specifically, we report turnover rates for the activation of the various types of C−H bonds in alkanes (normalized by their abundance) and relate them to their respective bond energies (Table 4). Even though the overall kinetics are governed by ROOH decomposition, the position of O-attachment in ROOH has already been determined in the ROOH formation step, so the ROOH decomposition step does not determine regioselectivity. Instead, we need to compare rate constant ratios for steps in which C−H bonds are activated to study the regioselectivity.

Activation energies for H-abstraction reflect those for reactions with ROO• for noncatalytic routes, because propagation occurs predominantly via step (v) in Scheme 1, ROO• + RH → ROOH + R•, and are controlled by C−H and O−H bond strengths in RH and ROOH, respectively,[5] in a manner consistent with linear-free energy relations.[43,44] We choose the above step based on the availability of data for this reaction and the absence of such data for reactions of bound ROO species. These relations[43,44] (line in Figure 9) and the C−H bond energies for primary (410 kJ/mol) and secondary (397 kJ/mol) C−H bonds can be used to estimate activation energies for O-insertion into each C−H bond and the ratio of rate constants for their activation (k_{prim}/k_{sec}). For *n*-hexane at 403 K, these k_{prim}/k_{sec} estimates are slightly larger (0.15) than measured values (0.10−0.11). High terminal selectivities reported earlier[14] would require k_{prim}/k_{sec} values ~20 times larger than predicted (Table 4). The similarities between k_{prim}/k_{sec} estimates and our measured values reflect the kinetic relevance of H abstraction by species with similar reactivity as ROO, whether present as adsorbed ROO in step (6), RO in step (2) of Scheme 2, or solvated ROO or RO radicals in the liquid phase. These reactivity ratios and terminal selectivities indicate that any spatial constraints on redox-active sites within MnAPO-18 channels do not induce regiospecificity in oxygen insertion pathways.

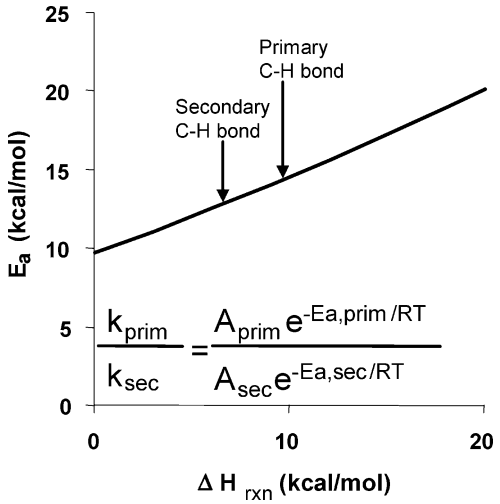

Figure 9. Linear free-energy relationship of activation energy vs enthalpy of reaction for ROO + RH → ROOH + R with inserted primary and secondary C−H bonds in hexyl groups.

Evans−Polanyi relations also can be used to estimate relative oxidation rates at the 2- and 3-positions in hexane. Our experimental selectivity patterns are identical on MnAPO-5 and MnAPO-18, consistent with the similar energies of these C−H bonds, and similar to those for noncatalytic autoxidation (Table 4). Secondary C−H bonds at the 2- and 3-positions are similar in energy (397 kJ/mol); oxygen insertion at the 2-carbon is slightly favored because of weaker steric constraints. A previous study claimed much higher O-insertion probabilities at the 3-position than at the 2-position for *n*-hexane on MeAPO-5 (e.g., 71% vs 16% on CoAPO-5, Table 3)[14] and no detectable O-insertion at the 1- and 2-positions for *n*-dodecane oxidation on MnAPO-5.[15] We have not found precedents or plausible mechanisms for these regioselectivity patterns, which may reflect inconsistencies in analytical protocols that may have also influenced the unprecedented selectivities and high oxidation rates reported for *n*-hexane oxidation on MeAPO-18 in these comparative studies.[14−16] We observe, as in previous studies,[6−9] similar rates of O-insertion at the 2- and 3-positions for both noncatalytic and catalytic oxidation of *n*-alkanes.

Regiospecificity Implications of Proposed Catalytic Sequence. Here, we examine specific strategies for improving terminal selectivities in alkane oxidation proceeding via the steps in Scheme 2.[25] Alkane−O_2 reactions on Mn and Co redox-active sites proceed via ROOH intermediates.[1,2] Redox-active Mn^{2+} and Co^{2+} sites decompose ROOH to form alcohols, ketones, and aldehydes as initial products,[21,45] which react further to form acids of varying chain length as secondary products. Turnover rates for ROH + R(−H)═O formation from cyclohexane on MeAPO-5, were proportional to ROOH concentration, consistent with ROOH intermediates.[25] These kinetic trends and conclusions are identical for the oxidation of *n*-hexane and cyclohexane[25] reactants. In the steps that form and decompose ROOH in Scheme 2, the location of oxygen insertion along the *n*-alkane backbone is determined by the steps in which RH enters the catalytic cycle. C−H bonds are activated in steps that form ROOH (step (6) in Scheme 2) and in reactions with RO* or OH* (steps (2) and (5)) within the ROOH decomposition cycle, as well as in parallel homogeneous routes involving ROO radicals solvated by the liquid phase.

Free radicals in Scheme 1 would be unable to participate in regiospecific C−H bond activation unless constrained within narrow channels and restricted from diffusing out of the crystallites; however, if products formed from the radical

reactions can diffuse out from the crystallites, free radicals are likely to do so as well leading to the normal free-radical C−H bond activation selectivities. Thus, only steps involving adsorbed species, such as those in Scheme 2, could detect any spatial constraints that favor regiospecific oxygen insertion. Preferential terminal selectivities would require that adsorbed species in steps (2), (5), and (6) of Scheme 2 react within environments that inhibit oxidation of nonterminal C−H bonds. Parallel noncatalytic autoxidation pathways, leading to unselective C−H bond activation, must be avoided, for instance, by minimizing [ROOH] concentrations in the extracrystalline liquid phase, because high ROOH concentrations favor noncatalytic over catalytic pathways. Previous studies of *n*-alkane activation using H_2O_2 (added or formed in situ)[7−9] and Cl_2[10−13] reported that structures with 10-membered rings gave modest terminal selectivities by allowing preferential activation of terminal C−H bonds. In a parallel study, we have used Mn-exchanged aluminosilicates with various pore sizes to probe the effects of spatial constraints on Mn-catalyzed *n*-hexane−O_2 pathways. Terminal selectivities were highest on 10-member ring zeolites with straight channels (MFI, 24%, $k_{prim}/k_{sec} = 0.42$)[46] reaching values similar to those reported on other zeolite catalysts.[7−9] These high selectivities were achieved with the additional presence of an acidic H-from of the zeolites, which acts as a scavenger of ROOH species present outside of Mn-containing channels. In this manner, we maintain a low ROOH concentration in the bulk liquid and favor primarily heterogeneous C−H bond activation and the effective use of spatial constraints provided by the inorganic scaffold containing redox-active sites.[46]

Conclusions

Hexanol and hexanal/hexanone synthesis rates were proportional to the hexyl hydroperoxide concentration and the number of Mn_{redox} sites for both MnAPO-5 and MnAPO-18, suggesting that the kinetically-relevant step involves decomposition of hexyl hydroperoxides on Mn_{redox} sites. This is similar to what is observed for cyclohexane oxidation on large-pore MnAPO-5, indicating that *n*-hexane and cyclohexane proceed via the same oxidation mechanism, involving formation and decomposition of alkyl hydroperoxide intermediates via bound radical-like intermediates. The similar hexyl hydroperoxide decomposition rates on MnAPO-18 and MnAPO-5 indicate that *n*-hexane reactants have ready access to both of these structures and that measured rates are kinetic in nature. Rapid *n*-hexane diffusion and adsorption into MnAPO-18 further supports the kinetic origin of measured rates. On the small-aperture MnAPO-18, cyclohexane oxidation turnover rates were 4.6 times lower than on MnAPO-5, because the smaller apertures on MnAPO-18 impose diffusional constraints on cyclohexane reactants. *n*-Hexane oxidation on both MnAPO-18 and MnAPO-5 led to oxygen introduction at all backbone positions, and a terminal selectivity (∼7%, $k_{prim}/k_{sec} = 0.11$) consistent with relative primary and secondary C−H bond energies in *n*-hexane and the absence of regioselective oxidation capability of the large intracrystalline cages in MnAPO-18 in contrast with a previous study.[14] The total selectivities to alkanoic acids are similar in both studies, although we primarily detect C_2−C_5 acids resulting from C−C bond breaking of the *n*-hexane backbone and only a small fraction of hexanoic acid resulting from terminal oxidation.

Acknowledgment. The authors acknowledge the financial support and the permission to publish these results from ExxonMobil Research and Engineering Co. We acknowledge Dr. Sebastian C. Reyes of ExxonMobil Research and Engineering Co. for carrying out the *n*-hexane uptake experiments. We thank Dr. Jay A. Labinger of the California Institute of Technology for the thoughtful comments that he provided during the review process, which led to a much improved manuscript. We thank Professor Robert G. Bergman of University of California, Berkeley for insightful suggestions on an earlier draft of the manuscript. We also thank Dr. Avelino Corma Canos of the Universidad Politécnica de Valencia for his advice and comments during the course of this study.

Supporting Information Available: The XRD pattern of MnAPO-18 and a typical GC chromatogram of *n*-hexane oxidation products are shown in the Supporting Information. This material is available free of charge via the Internet at http://pubs.acs.org.

References and Notes

(1) Sheldon, R. A.; Kochi, J. K. *Metal-Catalyzed Oxidations of Organic Compounds*; Academic Press: New York, 1981.
(2) Hill C. L. *Activation and Functionalization of Alkanes*; Wiley: New York, 1989.
(3) Batiot, C.; Hodnett, B. K. *Appl. Catal., A* **1996**, *137*, 179.
(4) Labinger, J. A. *J. Mol. Catal., A* **2004**, *220*, 27.
(5) McMillen, D. F.; Golden, D. M. *Ann. Rev. Phys. Chem.* **1982**, *33*, 493.
(6) Cook, B. R.; Reinert, T. J.; Suslick, K. S. *J. Am. Chem. Soc.* **1986**, *108*, 7281.
(7) Herron, N.; Tolman, C. A. *J. Am. Chem. Soc.* **1987**, *109*, 2837.
(8) Herron, N. *New J. Chem.* **1989**, *13*, 761.
(9) Tatsumi, T.; Watanabe, Y.; Hirasawa, Y. *Res. Chem. Intermed.* **1998**, *24*, 529.
(10) Turro, N. J.; Fehlner, J. R.; Hessler, D. P.; Welsh, K. M.; Ruderman, W.; Firnberg, D.; Braun, A. M. *J. Org. Chem.* **1988**, *53*, 3731.
(11) Turro, N. J.; Han, N.; Lei, X.-G.; Fehlner, J. R.; Abrams, L. *J. Am. Chem. Soc.* **1995**, *117*, 4881.
(12) Turro, N. J.; Fehlner, J. R. U.S. Patent 4,971,664, **1990**.
(13) Turro, N. J.; Fehlner, J. R. U.S. Patent 5,110,425, **1992**.
(14) Thomas, J. M.; Raja, R.; Sankar, G.; Bell, R. G. *Nature* **1999**, *398*, 227.
(15) Raja, R.; Thomas, J. M. *Chem. Commun.* **1998**, 1841.
(16) Raja, R.; Sankar, G.; Thomas, J. M. *J. Am. Chem. Soc.* **1999**, *121*, 11926.
(17) Thomas, J. M.; Raja, R.; Sankar, G.; Bell, R. G. *Stud. Surf. Sci. Catal.* **2000**, *130*, 887.
(18) Raja, R.; Sankar, G.; Thomas, J. M. *Angew. Chem., Int. Ed.* **2000**, *39*, 2313.
(19) Thomas, J. M.; Raja, R.; Sankar, G.; Bell, R. G. *Acc. Chem. Res.* **2001**, *34*, 191.
(20) Raja, R.; Thomas, J. M. *J. Mol. Catal., A* **2002**, *181*, 3.
(21) Labinger, J. A. *CATTECH* **1999**, *3*, 18.
(22) Hartmann, M.; Ernst, S. *Angew. Chem., Int. Ed.* **2001**, *39*, 888.
(23) Tian, P.; Xu, L.; Huang, T.; Xie, P.; Liu, Z. M. *Chem. J. Chin. Univ.* **2002**, *23*, 656.
(24) Moden, B.; Oliviero, L.; Dakka, J., Santiesteban, J. G.; Iglesia, E. *J. Phys. Chem. B* **2004**, *108*, 5552.
(25) Moden, B.; Zhan, B.-Z.; Dakka, J., Santiesteban, J. G.; Iglesia, E. *J. Catal.* **2006**, *239*, 390.
(26) Wilson, S. T.; Flanigen, E. M. U.S. Patent 4,567,029, **1986**.
(27) Chen, J. S.; Thomas, J. M. *J. Chem. Soc., Chem. Commun.* **1994**, 603.
(28) Barrett, P. A.; Sankar, G.; Catlow, C. R. A.; Thomas, J. M. *J. Phys. Chem.* **1996**, *100*, 8977.
(29) Cora, F.; Sankar, G.; Catlow, C. R. A.; Thomas, J. M. *Chem. Commun.* **2002**, 734.
(30) Chen, J. D.; Dakka, J.; Sheldon, R. A. *Appl. Catal., A* **1994**, *108*, L1.
(31) Beale, A. M.; Sankar, G.; Catlow, C. R. A.; Anderson, P. A.; Green, T. L. *Phys. Chem. Chem. Phys.* **2005**, *7*, 1856.
(32) Breck, D. W. *Zeolite Molecular Sieves*; Wiley: New York, 1974.
(33) Groves, J. T.; McClusky, G. A. *J. Am. Chem. Soc.* **1976**, *98*, 859.
(34) Russell, G. A. *J. Am. Chem. Soc.* **1957**, *78*, 3871.
(35) Chavez, F. A.; Rowland, J. M.; Olmstead, M. M.; Mascharak, P. K. *J. Am. Chem. Soc.* **1998**, *120*, 9015.
(36) Chavez, F. A.; Mascharak, P. K. *Acc. Chem. Res.* **2000**, *33*, 539.

(37) Hermans, I.; Nguyen, T. L.; Jacobs, P. A.; Peeters, J. *ChemPhysChem* **2005**, *6*, 637.
(38) Foster, M. D.; Rivin, I.; Treacy, M. M. J., Delgado Friedrichs, O. *Microporous Mesoporous Mater.* **2006**, *90*, 32.
(39) Tsonis, C. P. *Fuel Process. Technol.* **1988**, *17*, 285.
(40) Lin, M.; Hogan, T. E.; Sen, A. *J. Am. Chem. Soc.* **1996**, *118*, 4574.
(41) Kraushaar-Czarnetzki, B.; Hoogervorst, W. G. M.; Stork, W. H. J. *Stud. Surf. Sci. Catal.* **1994**, *84*, 1869.
(42) Sankar, G.; Raja, R.; Thomas, J. M. *Catal. Lett.* **1998**, *55*, 15.
(43) Denisov, E. T.; Denisova, T. G. *Handbook of Antioxidants*, 2nd ed.; CRC Press: Boca Raton, 2000.
(44) Denisova, T. G.; Denisov, E. T. *Russ. J. Phys. Chem.* **1987**, *61*, 1378.
(45) Black, J. F. *J. Am. Chem. Soc.* **1978**, *100*, 527.
(46) Zhan, B.-Z.; Moden, B.; Dakka, J., Santiesteban, J. G.; Iglesia, E., *J. Catal.* [Online early access], DOI: 10.1016/j.jcat.2006.10.019.